Particle Size Control of Cryptomelane Nanomaterials by Use of H_2O_2 in Acidic Conditions

Josanlet C. Villegas,[†] Luis J. Garces,[†] Sinue Gomez,[†] Jason P. Durand,[‡] and Steven L. Suib*[,†,‡,§]

Institute of Materials Science, Department of Chemistry, and Department of Chemical Engineering, University of Connecticut, 55 North Eagleville Road, Storrs, Connecticut 06269

Received September 16, 2004. Revised Manuscript Received January 20, 2005

A new soft-step chemistry method has been developed to prepare pure cryptomelane-type manganese oxide materials (OMS-2) with the smallest particle sizes ever reported. The synthetic procedure is based on the reduction of $KMnO_4$ by H_2O_2 under acidic conditions followed by reflux. An acetate-containing buffer solution and HNO_3 are used to control the pH of the reaction mixture. The formation process, particle size, crystallite size, crystal structure, and properties of these nanomaterials have been investigated by X-ray diffraction, scanning electron microscopy, high-resolution transmission electron microscopy (HRTEM), potentiometric titration, thermogravimetric analysis, and N_2 sorption analyses. Both the concentration of H_2O_2 and the nature of the acid used affect the crystalline phase formation, microstructure, thermal stability, and the composition of the final product. HRTEM images reveal that the OMS-2 nanofibers are not oriented preferentially and present significant twinning, along with discontinuity in the growth of the tunnel. Catalytic studies of these OMS-2 nanomaterials for oxidation of benzyl alcohol and fluorene have been performed. These nanomaterials show a low performance for the oxidation of benzyl alcohol and a unique catalytic activity for the oxidation of fluorene compared to OMS-2 materials prepared by conventional methods.

I. Introduction

Physical and chemical properties of materials are modified when they are present on a nanoscopic scale. This phenomenon makes nanomaterials promising for technological applications and opens up a completely new perspective for material design being the particle size a new powerful parameter.[1] One-dimensional (1D) nanoscale structures (nanorods, nanotubes, and nanofibers) have attracted interest in recent years due to their unique electronic, optical, mechanical, and magnetic properties and potential applications in many areas.[1−6] Methods to synthesize 1D nanoscale metal and semiconductor materials include template-directed,[7] photochemical processes,[5] laser ablation,[8] microemulsion,[9] and ion intercalation/deintercalation processes.[3]

Manganese oxide octahedral molecular sieves (OMS) are microporous materials consisting of mixed valence manganese oxides (Mn^{2+}, Mn^{3+}, and Mn^{4+}). The framework of these materials is made of edge- and corner-shared MnO_6 octahedra that form 1D tunnel structure.[10−13] Cryptomelane-type manganese oxide (OMS-2) is one group of the OMS family, containing 2×2 tunnel structure with a pore size of 4.6 Å. These materials have been widely used in separation, batteries, and catalysis.[12,14−17] Recently, OMS-2 has been reported as an easily regenerable catalyst for the acid-catalyzed, selective, and environmentally friendly oxidation of alcohols using air as an oxidant.[15] Extensive research has been done regarding the synthesis and properties of OMS-2 materials.[14,17−27] Various synthetic routes have been used to

* To whom correspondence should be addressed. E-mail: steven.suib@uconn.edu. Phone: 860-4862797. Fax: 860-4862981.
[†] Institute of Materials Science.
[‡] Department of Chemistry.
[§] Department of Chemical Engineering.

(1) Patzke, G. R.; Krumeich, F.; Nesper, R. *Angew. Chem., Int. Ed.* **2002**, *41*, 2446.
(2) Sun, Y.; Xia, Y. *Adv. Mater.* **2004**, *16*, 264.
(3) Ma, R.; Bando, Y.; Sasaki, T. *J. Phys. Chem. B* **2004**, *108*, 2115.
(4) Martin, C. R. *Science* **1994**, *266*, 1961.
(5) Liu, S.; Yue, J.; Gedanken, A. *Adv. Mater.* **2001**, *13*, 656.
(6) Xiong, Y.; Li, Z.; Zhang, R.; Xie, Y.; Yang, J.; Wu, C. *J. Phys. Chem. B* **2003**, *107*, 3697.
(7) (a) Lakshmi, B. B.; Patrisi, C. J.; Martin, C. R. *Chem. Mater.* **1997**, *9*, 2544. (b) Niederberger, M.; Krumeich, F.; Muhr, H. J.; Müller, M.; Nesper, R. *J. Mater. Chem.* **2001**, *11*, 1941.
(8) Morales, A. M.; Lieber, C. M. *Science* **1998**, *279*, 208.
(9) Guo, L.; Wu, Z.; Liu, T.; Wang, W.; Zhu, H. *Chem. Phys. Lett.* **2000**, *318*, 49.
(10) Clearfield, A. *Chem. Rev.* **1988**, *88*, 125.
(11) Post, J. E.; Burnham, C. W. *Am Miner.* **1986**, *71*, 1178.
(12) Suib, S. L. *Curr. Opin. Solid State Mater. Sci.* **1998**, 3, 63.
(13) Shen, Y. F.; Zerger, R. P.; DeGuzman, R. N.; Suib, S. L.; McCurdy, L.; Potter, D. I.; O'Young, C. L. *Science* **1993**, *260*, 511.
(14) (a) DeGuzman, R. N.; Shen, Y. F.; Shaw, B. R.; Suib, S. L.; O'Young, C. L. *Chem. Mater.* **1993**, *5*, 1395. (b) DeGuzman, R. N.; Shen, Y. F.; Neth, E. J.; Suib, S. L.; O'Young, C. L.; Levine, S.; Newsam, J. M. *Chem. Mater.* **1994**, *6*, 815.
(15) Son, Y. C.; Makwana, V. D.; Howell, A. R.; Suib, S. L. *Angew. Chem., Int. Ed.* **2001**, *40*, 4280.
(16) Krishman, V. V.; Suib, S, L. *J. Catal.* **1999**, *184*, 305.
(17) Luo, J.; Zhang, Q.; Huang, A.; Suib, S. L. *Microporous Mesoporous Mater.* **2000**, *35−36*, 209.
(18) Strobel, P.; Charenton, J. C. *Rev. Chim. Miner.* **1986**, *23*, 125.
(19) Chen, X.; Shen, Y. F.; Suib, S. L.; O'Young, C. L. *Chem. Mater.* **2002**, *14*, 940.
(20) Liu, J.; Makwana, V.; Cai, J.; Suib, S. L.; Aindow, M. *J. Phys. Chem. B* **2003**, *107*, 9185.
(21) Golden, D. C.; Dixon, J. B.; Chen, C. C. *Clays Clay Miner.* **1986**, *34*, 511.
(22) Golden, D. C.; Chen, C. C.; Dixon, J. B. *Clays Clay Miner.* **1987**, *35*, 271.
(23) Cai, L.; Liu, J.; Willis, W. S.; Suib, S. L. *Chem. Mater.* **2001**, *13*, 2413.

10.1021/cm048391u CCC: $30.25
Published on Web 03/11/2005

prepare OMS-2, such as oxidation of Mn^{2+} by $KMnO_4$, $K_2S_2O_8$, and O_2 in acidic solutions under refluxing conditions,[14,17−19] thermal or hydrothermal treatment of birnessites,[20−24] and a sol−gel route with the reaction between $KMnO_4$ and fumaric acid.[25,26] The reflux method involving the oxidation of Mn^{2+} by $KMnO_4$ is the most commonly used route to prepare bulk OMS-2 materials.

Synthesis of nanoscale OMS materials has raised scientific interest over the past few years due to the small particle size and high surface area of these materials. A wide variety of morphological forms of OMS, ranging from single crystals, thin films, and helices to nanowires, nanorods, and nanotubes, have been reported.[7a,28−33] Synthesis of OMS-2 fibers with particle size as small as 12.1 nm was achieved by Garces et al., by introducing poly(vinyl alcohol) (PVA) in the conventional synthesis procedure.[32] Liu et al. recently reported a novel sol−gel-assisted solid-state method to synthesize nanosized OMS-2 materials using cross-linking reagents.[33] The morphologies and sizes of these nanomaterials are controlled by the nature of the cross-linking agent used. However, even though this synthetic pathway shortened the time of preparation of nanoscale OMS-2, the particle size of the nanocrystal obtained ranged from 40 to 100 nm.

Here we report for the first time the synthesis of crystalline OMS-2 nanofibers with particle size as small as 6 nm without the use of template or cross-linking reagents. The synthetic procedure is based on the use of H_2O_2 to reduce MnO_4^- under acidic conditions to produce Mn^{2+} in situ, which reacts with excess of MnO_4^- in the media to form OMS-2. The particle size of the nanofibers is mainly controlled by the concentration of H_2O_2 in the reaction media. The new method developed eliminates the use of a Mn^{2+} source and also has the advantage that the only products of decomposition of H_2O_2 are H_2O and O_2, which makes the synthesis friendlier and also avoids the necessity of extensive washing and the use of calcination to remove any organic ions. This synthetic pathway not only simplifies the synthesis of OMS-2 nanomaterials but also reduces the reflux time from 24 h for the conventional preparation to about 15 h. The effects of the concentration of H_2O_2 and the acidity of the reaction mixture on the formation, properties, and crystal structure of the final products have been studied. The catalytic activity of OMS-2 nanomaterials in the oxidation reactions of benzyl alcohol and fluorene has also been investigated. The OMS-2 nanofibers prepared in this work show a unique catalytic activity if compared with other bulk OMS-2 prepared by conventional reflux methods.

II. Experimental Section

A. Synthesis. Nanoscale OMS-2 materials were prepared by using a reflux method for the reduction of Mn^{7+} by hydrogen peroxide under acidic conditions. This method involved a variation of the procedure used by Luo et al. for the preparation of synthetic cryptomelane.[17] In a typical synthesis, 40 mL of hydrogen peroxide (H_2O_2) solution 1% (v/v) was added to a buffer solution consisting of 5 mL of acetic acid and 5 g of potassium acetate in 40 mL of distilled−deionized water (DDW). A solution of 6.5 g of $KMnO_4$ in 150 mL of DDW was then added dropwise to the above mixture while stirring. The resulting solution was refluxed for 24 h, and the product was filtered, washed, and dried in air at 80 °C overnight to remove water and then dried at 120 °C for 2 h. The OMS-2 obtained this way is called OMS-2 (1). The concentration of the H_2O_2 solution in the synthesis was varied between 0.25 and 15% (v/v). Standard OMS-2 was also prepared on the basis of this synthesis for comparison purposes. A solution of manganese acetate instead of H_2O_2 was used during the preparation as it is described elsewhere.[17,32]

To investigate the effect of the nature of the acid in the reaction media in the crystalline formation process, crystallite size, and particle size, OMS-2 materials were prepared from $KMnO_4$ and H_2O_2 using nitric acid (HNO_3) instead of the buffer solution. Hydrogen peroxide solution (30 mL) with concentrations of 1, 5, 10, and 15% and 3 mL of concentrated HNO_3 were used for the synthesis. The molar ratio of salt and H_2O_2 was adjusted to be the same as in the above procedure. OMS-2 materials obtained with this synthetic procedure are called OMS-2 (H*x*), where *x* stands for the concentration of H_2O_2 used in units of percentage.

B. Characterization. Powder X-ray diffraction (XRD) studies were performed with a Scintag XDS-2000 diffractometer using Cu Kα radiation and with a beam voltage of 45 kV and 40 mA of beam current. The data were collected in the 2θ range 5−70° with a continuous scan rate of 2°/min and the phases were identified using a JCPDS database. Crystalline particle size of the prepared materials was determined by using the Scherrer equation. The crystallite size reported is the average of the values obtained by applying Scherrer's equation to the diffraction peaks at $2\theta = 28.8$ (310) and 49.8° (411). The instrumental line broadening was corrected using a LaB_6 standard.

The morphology was studied by field emission scanning electron microscopy (FESEM) on a Zeiss DSM 982 Gemini FESEM with a Schottky Emitter at an accelerating voltage of 2 kV and a beam current of about 1 μA. Transmission electron microscopy (TEM) images were obtained using a JEOL 2010 FasTEM 200 kV instrument equipped with an EDAX energy dispersive spectrometer and a Gatan EELS/GIF system. Samples for analysis by TEM were prepared by placing a drop of a suspension containing powder OMS-2 in 2-propanol on a holey carbon-coated copper grid.

The average oxidation state (AOS) of manganese was determined by potentiometric titration methods.[34] Specific surface area measurements were performed at 77 K with a Micromeritics ASAP 2010 accelerated surface and porosimetry system. The samples were previously degassed at 120 °C for 12 h. The surface area of the samples was measured using the Brunauer−Emmett−Teller (BET) method.

(24) (a) Giovanoli, R.; Balmer, B. *Chimia* **1981**, *35*, 53. (b) Giovanoli, R.; Faller, M. *Chimia* **1989**, *43*, 54.
(25) Ching, S.; Roark, J. L.; Duan, N.; Suib, S. L. *Chem. Mater.* **1997**, *9*, 750.
(26) Duan, N.; Suib, S. L.; O'Young, C. L. *J. Chem. Soc. Chem. Commun.* **1995**, *13*, 1367.
(27) Feng, Q.; Kanoh, H.; Miyai, Y.; Ooi, K. *Chem. Mater.* **1995**, *7*, 148.
(28) (a) Brock, S. L.; Sanabria, M.; Suib, S. L. *J Phys. Chem. B* **1999**, *103*, 7416. (b) Giraldo, O.; Brock, S. L.; Marquez, M.; Suib, S. L.; Hillhouse, H.; Tsapatsis, M. *Nature* **2000**, *405*, 38. (c) Giraldo, O.; Marquez, M.; Brock, S. L.; Suib, S. L., Hillhouse, H.; Tsapatsis, M. *J. Am. Chem. Soc.* **2000**, *122*, 12158.
(29) Wang, X.; Li, Y. *J. Am. Chem. Soc.* **2002**, *124*, 2880.
(30) Xia, G. G.; Tong, W.; Tolentino, E. N.; Duan, N. G.; Brock, S. L.; Wang, J. Y., Suib, S. L. *Chem. Mater.* **2001**, *13*, 1585.
(31) Sugantha, M.; Ramakrishnan, P. A.; Hermann, A. M.; Warmsingh, C. P.; Ginley, D. S. *Int. J. Hydrogen Energy* **2003**, *28*, 597.
(32) Garces, L. J.; Hincapie, B.; Makwana, V. D.; Laubernds, K.; Sacco, A.; Suib, S. L. *Microporous Mesosporous Mater.* **2003**, *63*, 11.
(33) Liu, J.; Son, Y. C.; Cai, J.; Shen, X.; Suib, S. L.; Aindow, M. *Chem. Mater.* **2004**, *16*, 276.
(34) Glover, D.; Schumm, B., Jr.; Kozowa, A. *Handbook of Manganese Dioxides Battery Grade*; International Battery Materials Association: Cleveland, OH, 1989.

Thermogravimetric analyses (TGA) were done on a Hi-Res TGA 2950. The experiments were conducted under N_2 atmosphere at a temperature ramp of 10 °C/min. Thermal stability of the materials was also studied by temperature programmed desorption combined with a mass spectrometer (TPD-MS). About 30−40 mg of the sample was packed into a quartz tube and loaded into a tubular furnace. The sample was purged with He for 6 h at room temperature followed by heating to 700 °C at 10 °C/min. The evolved gases (water, oxygen, and carbon dioxide) were monitored with a MKS-UTI PPT quadrupole mass spectrometer.

C. Catalytic Applications. Catalytic applications were explored for the oxidation of benzyl alcohol and fluorene. The performance of the nanoscale OMS-2 (1) was compared with that of the conventional OMS-2 prepared by reflux. Prior to the reaction, OMS-2 catalysts were ion exchanged with H^+ to give the acid form, H−K−OMS-2, using a method described elsewhere.[35] Both catalysts were dried at 400 °C overnight before the catalytic reaction to eliminate moisture and any traces of nitrate or acetate. The oxidation of benzyl alcohol to benzaldehyde was performed using a method reported by Makwana et al.[35] Briefly, 15 mL of toluene, 1 mmol of the alcohol, and 0.5 mmol of methyl benzoate were added to a round-bottom flask. Then, 0.05 g of the catalyst was added and the mixture was stirred under reflux at 110 °C for 4 h. For the catalytic oxidation of fluorene, a batch reactor was also used in which 25 mL of isooctane, 6.6 mmol of fluorene, and 0.25 g of catalyst were loaded. The mixture was stirred under reflux at 80 °C for 8 h. OMS-2 catalysts were removed by filtration. The filtrate was analyzed using gas chromatography/mass spectrometry (GC/MS) and ^{1}H NMR.

III. Results

Formation of K−OMS-2. When $KMnO_4$ is added to a solution of H_2O_2 in the presence of nitric acid or buffer solution, the system remains clear for a period of time which depends on the initial concentration of H_2O_2 used. As the addition of permanganate proceeds, the system turns light brown and finally a brownish precipitate is observed. Upon completion of mixing the reactants, a poorly ordered manganese oxide (MnO_x) phase is obtained. The transformation of this phase to OMS-2 with time was followed by XRD. Figure 1a shows the XRD patterns of OMS-2 (1) at different reflux times. At a reflux time of 1 h, four reflections are observed, which increase in intensity up to 7.5 h. As the reflux time increases, the intensities of these peaks gradually decrease and characteristic XRD peaks of OMS-2 begin to appear. Pure OMS-2 is observed after 18 h of reflux.

The reflux time required to convert the initial MnO_x phase to OMS-2 varies with the concentration of H_2O_2 used. As the amount of H_2O_2 in the initial reactant mixture increases, the OMS-2 formation time decreases. For instance, OMS-2 is formed after 7.5 h of reflux when 5% of H_2O_2 is used.

The XRD patterns obtained at different reflux times for the OMS-2 (1H) sample are depicted in Figure 1b. As in the case of OMS-2 (1), a poorly ordered MnO_x phase is observed at $t = 0$ h. However, diffraction peaks of birnessite are observed after 1 h of reflux. These peaks become more intense as the reflux time goes from 1 to 3 h. After this time, the intensity of the birnessite peak decreases and diffraction peaks corresponding to cryptomelane begin to appear. Birnessite disappears at 7.5 h of reflux.

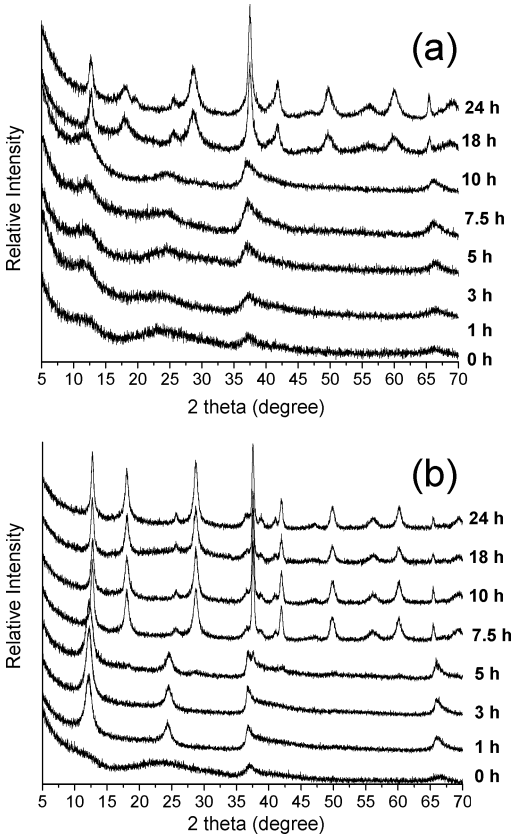

Figure 1. XRD patterns of OMS-2 prepared using 1% (v/v) solution of H_2O_2 at different reflux times with (a) buffer solution, OMS-2 (1), and (b) HNO_3, OMS-2 (1H).

XRD was also used to study the influence of the concentration of H_2O_2 solution on the crystallization of the cryptomelane phase. Figure 2 shows XRD patterns of OMS-2 prepared at different concentrations of H_2O_2 using buffer solution (Figure 2a) or HNO_3 (Figure 2b). The X-ray pattern of OMS-2 prepared by the conventional redox method using buffer solution is also shown in Figure 2a. Samples synthesized using H_2O_2 solution with concentrations between 0.25 and 5% show a pure cryptomelane phase pattern (Figure 2a). However, differences in the widths and intensities of the peaks are observed. OMS-2 prepared by the conventional method has the highest intensities and narrowest peaks. Cryptomelane peaks become broader as the percentage of H_2O_2 in the initial reaction mixture increases, which is associated with a decrease in crystallite size. Also, as the concentration of H_2O_2 increases, the intensities of these peaks decrease significantly and new intense and narrow peaks appear when the percentage of H_2O_2 used is higher than 5%. This new phase represents the majority of the crystalline phase and corresponds to manganite (γ-MnOOH, JCPDS 41-1379).

The effect of the nature of the acid used in the synthesis on the crystallization of OMS-2 nanomaterials was also studied. HNO_3 was used instead of the buffer solution to vary the pH of the reaction medium from 4.5 to 2. XRD patterns of OMS-2 prepared at pH = 2 revealed that a pure cryptomelane phase is formed in all the range of H_2O_2 concentrations studied (Figure 2b). OMS-2 (1H) shows the

(35) Makwana, V. D.; Garces, L. J.; Liu, J.; Cai, J.; Son, Y. C.; Suib, S. L. *Catal. Today* **2003**, *85*, 225.

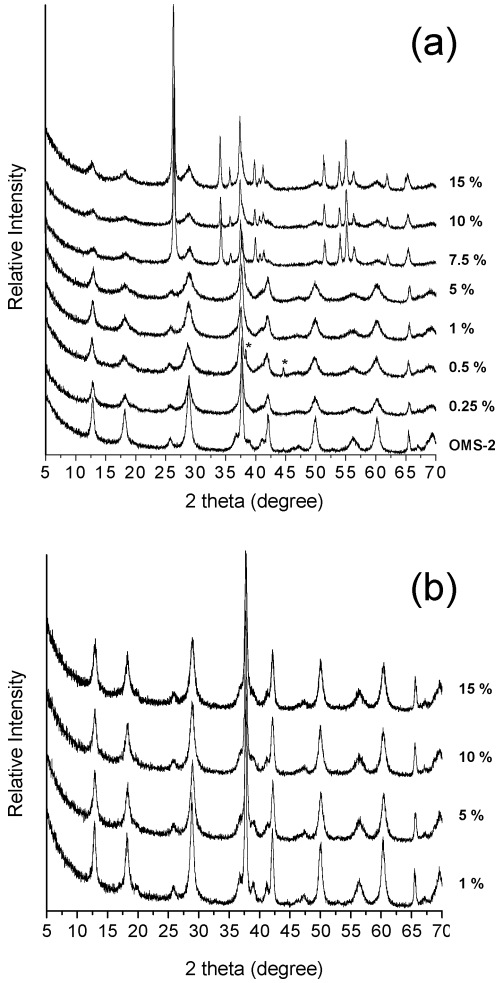

Figure 2. XRD pattern of OMS-2 nanomaterials prepared at different concentrations of H_2O_2 using (a) buffer solution and (b) HNO_3 (Al sample holder).

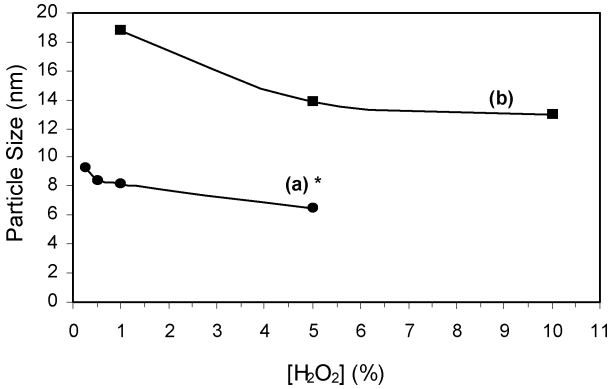

Figure 3. Effect of the concentration of H_2O_2 solution and the nature of the acid used in the reaction medium on the particle size of OMS-2 materials. Curve a corresponds to the OMS-2 prepared using buffer solution, and curve b corresponds to OMS-2 obtained using HNO_3. (The pure OMS-2 phase is not obtained at concentration of H_2O_2 greater than 5%.)

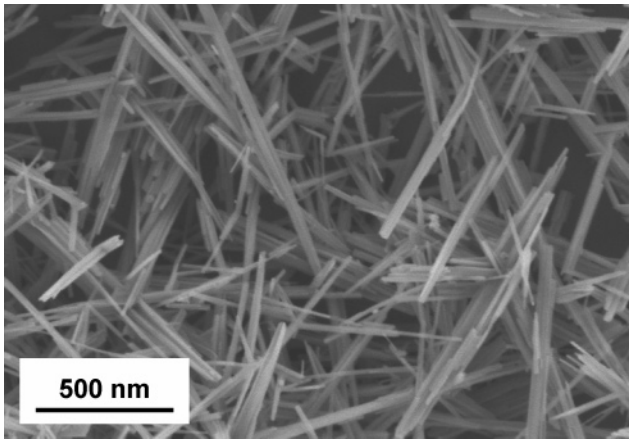

Figure 4. FESEM image of the morphology of OMS-2 (1) prepared using buffer solution and 1% H_2O_2 solution.

most intense and narrowest peaks, indicating that this material is highly crystalline. As observed in Figure 2a, the intensities of the diffraction peaks in Figure 2b decrease with increasing of H_2O_2 content in the reaction media. An increase in the widths of the peaks is also observed. However, the line broadening observed in the XRD patterns of these materials is not as pronounced as that for buffer-synthesized OMS-2 materials, as evidenced by the presence of less intense diffraction peaks at $2\theta = 41$ and 47°.

The variation in peak broadening with the amount of H_2O_2 in all the synthesized materials revealed differences in crystal size. Figure 3 presents the sizes of OMS-2 crystals prepared with different concentrations of H_2O_2 calculated from line broadening of XRD peaks using Scherrer's equation. The crystallite size decreases in all the samples as the amount of H_2O_2 in the synthesis increases. OMS-2 prepared with buffer solution has smaller crystallite sizes than those obtained with HNO_3. OMS-2 (1) has a crystallite particle size of 8.2 nm, while OMS-2 (1H) has a crystallite size of 18.8 nm. The same behavior is observed when 5% H_2O_2 solution was used.

The formation of OMS-2 materials was also corroborated by AOS measurements. The AOS of Mn for all the manganese oxide materials prepared at different concentrations of H_2O_2 and at different initial pH values are listed in Table 1. The AOS of the synthesized OMS-2 materials varies

Table 1. AOS of Mn of K−OMS-2 Nanomaterials Prepared Using Different Concentrations of H_2O_2 and Different pH

samples	AOS ± 0.03
K−OMS-2 (0.25)	3.87
K−OMS-2 (0.5)	3.80
K−OMS-2 (1)	3.75
K−OMS-2 (5)	3.69
K−OMS-2 (7.5)	3.46
K−OMS-2 (10)	3.41
K−OMS-2 (15)	3.36
K−OMS-2 (1H)	3.90
K−OMS-2 (5H)	3.84
K−OMS-2 (10H)	3.76

from 3.77 to 3.90. These values are in agreement with the AOS of Mn reported in the literature for K−OMS-2.[12] The oxidation state of Mn decreases as the reducing agent increases. Samples prepared using HNO_3 show AOS values slightly higher than their counterpart prepared using buffer solution. The AOS of Mn for samples prepared with buffer solution decreases from 3.84 to 3.36 when concentration of H_2O_2 varies from 5 to 15%. This indicates that Mn^{3+} species are present in this sample in larger amounts than in the OMS-2 prepared using H_2O_2 concentrations between 0.25 and 5%.

FESEM and TEM studies. The FESEM micrograph (Figure 4) shows the morphology of sample OMS-2 (1). OMS-2 nanomaterials prepared at H_2O_2 concentration other

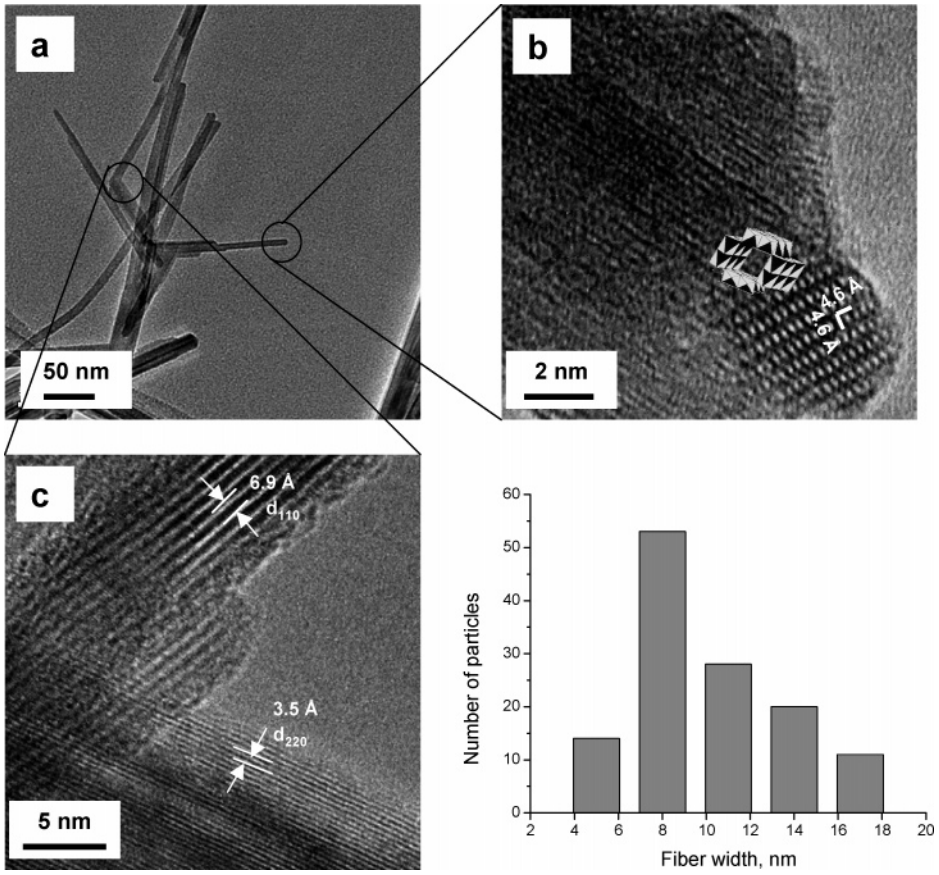

Figure 5. HRTEM micrograph and fiber width distribution (sample size 130 fibers) of OMS-2 (1) nanomaterials.

that 1% have a similar morphology. The materials consist of fibers or needlelike particles with widths of a few tens of nanometers, which varies depending on the concentration of H_2O_2. Similar fibrous morphology has been observed for bulk and nanoscale OMS-2 prepared by reflux.[19,32] The lengths of the nanofibers vary from a few hundred nanometers to several tens of micrometers. OMS-2 nanofibers prepared using HNO_3 are more uniform in length than those prepared at the same concentration of H_2O_2 using buffer solution.

The crystal structure of nanosized OMS-2 was studied using TEM. Figure 5 shows the typical HRTEM micrographs and fiber width distribution of the OMS-2 nanofibers. The fiber morphology is represented in Figure 5a. The fiber width distribution is depicted in Figure 5d; the width of the nanofibers is in the 4.0−18.0 nm range, with an average size of 9.8 nm and a standard deviation of 4.0 based on the count of 130 particles. The fiber widths obtained by TEM for these materials are similar to the crystallite sizes obtained from XRD.

HRTEM images show that the majority of the fibers lie on the (110) plane. However, some of the fibers have other planes exposed on the surface. In Figure 5c, we can observe in one fiber the lattice fringes separated by 6.9 Å, which correspond to the (110) plane, while in other fiber the (220) fringes with a separation of 3.5 Å are observed. The distance between lattice planes is consistent with that of the bulk, measured by XRD. On the other hand, Figure 5b shows the 2×2 tunnel structure of OMS-2 exposed at the end of one fiber.

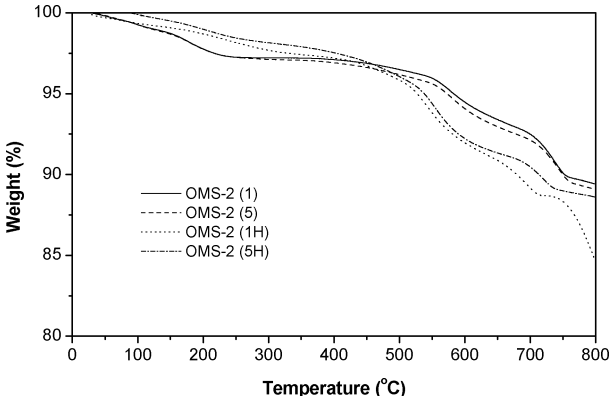

Figure 6. TGA profile for OMS-2 nanomaterials prepared at concentrations of H_2O_2 of 1 and 5% using buffer solution and HNO_3.

Thermal Stability. Thermal stability of K−OMS-2 nanomaterials synthesized with buffer solution or HNO_3 using 1 and 5% H_2O_2 was studied using TGA and TPD under inert atmosphere. The TGA curves for OMS-2 (1), OMS-2 (5), OMS-2 (1H), and OMS-2 (5H) are shown in Figure 6. Samples prepared using buffer solution or HNO_3 do not show a significant change in the TGA profile with the variation of H_2O_2 from 1 to 5%. This indicates that the thermal stability of these nanomaterials is not affected by the amount of H_2O_2 used in the synthesis. OMS-2 materials prepared at the same concentration of peroxide but at different acidic conditions show a variation in the TGA curves. OMS-2 materials synthesized with the buffer solution (OMS-2 (1) and OMS-2 (5)) are thermally more stable than their homologous OMS-2 (1H) and OMS-2 (5H) prepared with HNO_3.

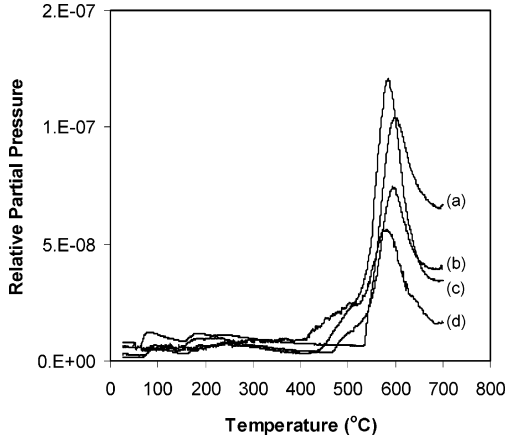

Figure 7. TPD of O_2 of OMS-2 nanomaterials prepared at concentrations of H_2O_2 of 1 and 5% using buffer solution and HNO_3. (a) OMS-2 (1); (b) OMS-2 (5); (c) OMS-2 (1H); OMS-2 (5H).

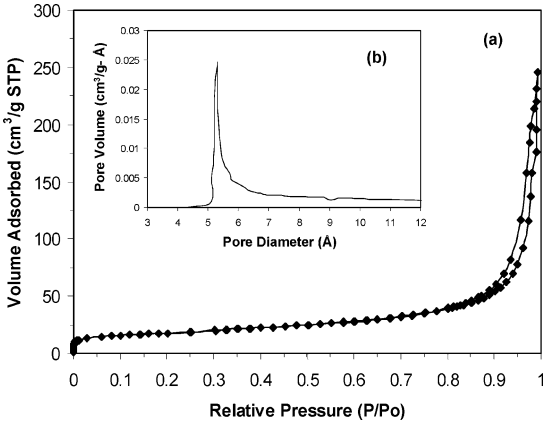

Figure 8. (a) N_2 adsorption/desorption isotherm of OMS-2 (1) nanomaterials; (b) Horvath−Kawazoe pore size distribution curve of OMS-2 (1).

From the TGA profile for OMS-2 (1) and OMS-2 (5) it can be seen that there are three major weight losses. The first weight loss (∼3%) is in the range of 100−240 °C and is due to water physically adsorbed on the surface of the material, consistent with the observation in the H_2O TPD. The second TGA weight loss is about 3% for OMS-2 (1) and 4% for OMS-2 (5) in the range of 400−610 °C. The last weight loss (4%) is observed from 610 to 760 °C. Similar thermal behavior has been previously reported for OMS-2.[19,20] The range of weight losses varies depending on the synthetic procedure. Weight losses occurring in the range of 300−650 °C have been attributed to the evolution of chemically adsorbed water and oxygen species from the material. The last TGA weight loss has been assigned to the evolution of structural oxygen in the framework of the tunnels.[19,20]

From TGA data for OMS-2 (1H) and OMS-2 (5H) (Figure 6), the first weight loss occurs in a large range of temperatures (from 100 to 315 °C) and is about 3 and 2%, respectively. A large amount of weight loss (∼7%) takes place in the range of 360−600 °C, corresponding to the evolution of water and removal of oxygen species, as detected in the H_2O and O_2 TPDs, respectively. At 600 °C, the weight of the samples continues decreasing until the temperature reaches 720 °C. The weight loss at this temperature is about 4% for OMS-2 (1H) and 2% for OMS-2 (5H). At temperatures higher than 720 °C, OMS-2 (1H) shows a marked decrease in weight.

The evolution of oxygen from OMS-2 (1), OMS-2 (5), OMS-2 (1H), and OMS-2 (5H) as a function of temperature is depicted in Figure 7. The small peaks observed in the range of 70 to 200 °C are due to desorption of water, as observed in the TPD data. This indicates that the pretreatment was not enough to eliminate the physically adsorbed water. The small and strong peaks observed between 400 and 650 °C are due to the atomic oxygen species and lattice oxygen, respectively.[35,36] As the acidity of the reaction media changes from pH 2 to 4.5, these peaks shift to higher temperatures. The strong oxygen peak for OMS-2 nanomaterials prepared at pH = 2 is located at 585 °C, while OMS-2 (1) and OMS-2 (5) synthesized at pH = 4.5 have this peak at 600 °C. The intensity of the oxygen peaks is a measure of the availability of the O_2 species in specific temperature regimes. As observed in Figure 7, the relative intensities of the peaks vary with percentage of H_2O_2.

Table 2. BET Surface Areas (S_{BET}), Total Pore Volume (V_p), and Micropore Volume (V_{mic}) of K−OMS-2 Nanomaterials

samples	S_{BET} (m2/g)	V_p (cm^3/g)	V_{mic} (cm^3/g)
K−OMS-2 (0.25)	64	0.3021	0.0057
K−OMS-2 (0.5)	71	0.2952	0.0026
K−OMS-2 (1)	62	0.3800	0.0041
K−OMS-2 (5)	64	0.3109	0.0058
K−OMS-2 (1H)	32	0.1223	0.0054
K−OMS-2 (5H)	42	0.1426	0.0012
K−OMS-2 (10H)	41	0.0828	0.0055

Textural Properties. The N_2 adsorption/desorption isotherm and the pore size distribution of OMS-2 (1) nanomaterials are shown in Figure 8. The isotherms recorded for all pure OMS-2 nanomaterials are similar to this and correspond to the type II adsorption isotherms (IUPAC classification)[37] with microporous filling at low P/P_0 and capillary condensation at high P/P_0. OMS-2 materials prepared using a conventional reflux method also exhibit this type of isotherm.[19] Pore size distribution curves of the pure OMS-2 nanomaterials prepared using the new synthetic route reported in this paper are also similar to those obtained for conventional OMS-2.[19] All the nanomaterials exhibit a narrow peak in the range of 4.8−5.3 Å pore diameter, as observed in Figure 8 for OMS-2 (1), which reveals the microporous structure of the samples. However, the contribution of the micropores to the total pore volume of the samples is not significant as shown in Table 2. The average pore diameter of the prepared samples ranges from 100 to 245 Å, suggesting the existence of mesoporous in the samples. These mesoporous samples contribute to a large extent to the total pore volume of the samples and according to previous work they consist of slit-shaped pores with nonuniform sizes or shapes.[19]

(36) (a) Yin, Y. G.; Xu, W. Q.; DeGuzman, R.; Suib, S. L. *Inorg. Chem.* **1994**, *33*, 4384. (b) Yin, Y. G.; Xu, W. Q.; Shen, Y. F.; Suib, S. L.; O'Young, C. L. *Chem. Mater.* **1994**, *6*, 1803.

(37) Sing, K. S. W.; Everett, D. H.; Haul, R. A. W.; Moscou, L.; Pierotti, R. A. Rouquérol, J.; Siemieniewska, T. *Pure Appl. Chem.* **1985**, *57*, 603.

The BET surface areas of K−OMS-2 nanomaterials prepared with different concentrations of peroxide and at different pH are also shown in Table 2. The surface areas of the buffer-synthesized OMS-2 materials are higher than those obtained from the corresponding OMS-2 materials prepared at the same concentration of H_2O_2 but using HNO_3.

Catalytic Activity of OMS-2 Nanofibers. Bulk OMS-2 and H−K−OMS-2 have been used as catalysts in the oxidation of benzyl alcohol to benzaldehyde showing a conversion higher than 90%.[15,35] The catalytic performance of OMS-2 nanomaterials was explored in the oxidation of benzyl alcohol. The acid form of the nanoscale OMS-2 (1) material was the catalyst used for this oxidative reaction. H−K−OMS-2 (1) showed 100% selectivity to benzaldehyde, but the conversion was lower compared with bulk OMS-2, only 16%. Nanoscale H−K−OMS-2 (1) and bulk OMS-2 materials were also used for the oxidation of fluorene. Contrary to the oxidation of benzyl alcohol, OMS-2 nanomaterials showed unique catalytic activity for the oxidation of fluorene to 9-fluorenone. The conversion of the oxidative reaction using H−K−OMS-2 (1) nanomaterials was 99% after 8 h of reaction, whereas the conversion using bulk H−K−OMS-2 was 19%.

IV. Discussion

Formation and Crystallization of OMS-2 Nanomaterials. OMS-2 materials were prepared by a soft-step chemistry route, through the reduction of Mn^{7+} by H_2O_2 under acidic conditions. In acidic solutions, H_2O_2 essentially reduces higher valence Mn species to Mn^{2+}.[38−41] The permanganate reduction in the presence of H_2O_2 is especially fast, as indicated by the disappearance of the purple color of this solution while the system turns pale pink. The intensity of the pink color depends on the initial concentration of H_2O_2 in the medium. When the percentage of H_2O_2 used in the mixture is less than 5% the pink color is rarely observed and the system remains transparent. As the concentration of H_2O_2 increases, more Mn^{7+} species are reduced to Mn^{2+}, resulting in higher concentration of these lower valence Mn species in the reaction medium, and thus a pale pink color is observed.

As the addition of $KMnO_4$ proceeds, the system turns brownish and precipitates are observed, indicating the beginning of the formation of solid MnO_x. Initially, MnO_x was formed just from the redox reaction occurring between the Mn^{2+} ions formed in situ and the excess of permanganate. However, the reaction between higher valence Mn species and H_2O_2 is not that simple. Kinetic studies have been conducted to understand the mechanism of this reaction, and different pathways have been proposed.[39−42] In general, these investigations have suggested that in acidic solutions reactions such as formation of peroxide complexes with Mn(II) or Mn(III),[40,41] reoxidation of Mn^{2+},[39] autocatalytic reaction of Mn^{2+},[41] among others, can occur and play an important role on product distribution.

OMS-2 nanomaterials are formed through the transformation of a lamellar phase, which is obtained after the reaction between $KMnO_4$ and H_2O_2 as indicated by XRD studies (Figure 1). In the case of OMS-2 prepared using buffer solution the transformation occurs from a poorly ordered birnessite-like material (Figure 1a), while if HNO_3 is used OMS-2 materials are obtained from well-crystallized birnessites, as shown in Figure 1b for OMS-2 (1H) sample. The reflux time required to convert the lamellar phase to cryptomelane-type phase varies with the concentration of H_2O_2 used. An increase in the concentration of H_2O_2 results in an increase in the amount of Mn^{2+} ions in the medium, causing an increment in the rate of the reaction. The effect of H_2O_2 on the reaction rate has been previously reported by Casado et al.[41] As mentioned above, Mn^{2+} ions have an autocatalytic effect on the reaction. This effect is accelerated by the higher concentration of Mn^{2+} ions in the medium. Because of the acceleration of the reaction rate, the layered manganese oxide phase is formed in an earlier stage of the reaction, which gives time to the material to get a certain range of order before the beginning of the reflux. This is consistent with XRD studies where an ordered phase is observed at earlier reflux times as the concentration of H_2O_2 increases, resulting in a rapid transformation to cryptomelane-type phase. OMS-2 nanomaterials synthesized using the buffer solution and 1% H_2O_2 solution are formed after 10 h of reflux (Figure 1a), while 7.5 h are only needed if the concentration of H_2O_2 increases to 5%.

The influence of H_2O_2 and the nature of the acid used on the crystallization of OMS-2 nanomaterials were investigated by comparing XRD patterns of the materials prepared at different concentrations of H_2O_2 and both acid systems after 24 h of reflux (Figure 2). X-ray patterns for the samples synthesized using buffer solution show that pure OMS-2 phase can be obtained in the range of H_2O_2 from 0.25 to 5%. A greater amount of peroxide results in a vigorous reduction of permanganate and in the formation of not only OMS-2 but also manganite, γ-MnOOH, in the material, as observed in Figure 2a. The presence of manganite in the materials was also corroborated by FESEM and AOS measurements (Table 1). OMS-2 (7.5), OMS-2 (10), and OMS-2 (15) samples have manganese AOS values of 3.46, 3.41, and 3.36, respectively, which suggest that more Mn^{3+} relative to Mn^{4+} is present in these samples. Since a substitution of Mn^{4+} is not possible under these synthetic conditions, the AOS values closer to 3 in these materials are due to the presence of the manganite as the majority of the crystalline phase.

When HNO_3 is used to decrease the pH of the reaction medium, a pure OMS-2 phase is obtained in all the range of H_2O_2 concentrations studied, as evidenced by XRD studies and AOS measurements (Figure 2b and Table 1). This result suggests that although the amount of peroxide used influence the reducing power of the reaction, as was mentioned above,

(38) Broughton, D. B.; Wentworth, R. L. *J. Am. Chem. Soc.* **1947**, *69*, 741.
(39) Baral, S.; Lume-Pereira, C.; Janata, E.; Henglein, A. *J. Phys. Chem.* **1985**, *89*, 5779.
(40) Jacobsen, F.; Holcman, J.; Sehested, K. *Int. J. Chem. Kinet*. **1998**, *30*, 207.
(41) (a) Casado, J.; Lizaso-Lamsfus, J. *Anal. Real Soc. Esp. Fis. Quim.* **1967**, *63*, 739. (b) Senent, S.; Casado, J.; Lizaso, J. *Anal. Real Soc. Esp. Fis. Quim.* **1971**, *67*, 1133.
(42) Lin, Z. X.; Huang, T. T. *Ind. Eng. Chem. Res.* **1987**, *26*, 2148.

the presence of nitric acid in the medium also affects the reaction and has an important role in determining the composition of the product. Since nitrates have an oxidative nature, these groups could oxidize Mn^{2+} species to higher oxidation states, diminishing the concentration of Mn^{2+} in the medium and though an autocatalytic effect. Therefore, this system has less reducing power than the system containing acetate groups (buffer solution). The lower pH of the medium could also cause the disproportionation of Mn^{3+} species to Mn^{4+} and Mn^{2+}, avoiding the formation of manganite.

Effect of Concentration of H_2O_2 and pH on the Particle Size of OMS-2 Nanomaterials. The crystallite sizes and fiber diameters (particle size) of the OMS-2 nanomaterials were also affected by the initial amount of H_2O_2, as evidenced by XRD line broadening results (Figure 3) and electron microscopy (Figure 5), respectively. Particle sizes of all synthesized OMS-2 materials decrease with an increase of the H_2O_2 concentration in the medium. This behavior is due to the dependence of the reaction rate on the H_2O_2 percentages in the synthesis medium. An increase in the H_2O_2 concentration produces an increase of the reaction rate, which will accelerate the crystallization process, limiting the particle growth and reducing the particle size of the material. This conclusion is also supported by the fact that conventional OMS-2 prepared using a Mn^{2+} source and that the buffer solution has a crystallite size of 29.8 nm,[32] which is reduced to 9.3 nm when a solution of 0.25% of H_2O_2 is incorporated in the synthesis to produce Mn^{2+} in situ.

The difference in particle size obtained for the samples prepared at the same H_2O_2 concentration but changing the nature of the acid is probably related to the presence of acetate groups in the buffer solution. Carbonyl groups in the buffer solution may have formed bonds with the surface OH groups on the manganese oxide materials, causing the isolation manganese oxide particles from each other by the surrounding acetate groups and preventing further aggregation. The influence of acetate on the particle size has been previously reported in the synthesis of zinc sulfide particles.[43] The formation of nanometer-sized ZnS particles has been ascribed to a complexing-attachment phenomena of the ZnS particles with acetate anions.

Morphology and Crystal Structure. Synthetic OMS-2 materials show the typical fibrous morphology of cryptomelane-type materials (Figures 4 and 5). A closer examination of the samples reveals that the width of these fibers is a few hundred nanometers. Depending on synthesis conditions, fibers with dimensions smaller than those reported in the literature for other nanosized OMS-2 materials[32,33] can be obtained. The shape of the OMS-2 nanofibers prepared at pH = 4.5 seems to be more needlelike rather than a round cylinder, as evidenced by FESEM images.

HRTEM reveals that the majority of OMS-2 nanofibers are oriented on a preferential plane and show discontinuity in the growth of the tunnels. Extensive twinning and defective crystals have been observed in layered materials prepared by conventional methods.[22,44] At earlier stages of the synthetic process reported in this work a poorly crystalline layered phase is observed, which slowly transforms to the OMS-2 tunnel structure, as observed by XRD. Layered manganese oxide structures are formed by edge-shared MnO_6 octahedra containing Mn^{4+} and Mn^{3+}. During the transformation process from layered structure to tunnel structure, some of the Mn^{3+} octahedra from the layer migrates as a corner-sharing octahedra to intervene in the formation of the tunnels.[20] Thus, the migration of the Mn^{3+} octahedra from the poorly ordered layered precursor may interact with other neighbor octahedra to form the tunnels, which would result in defective nanoparticles with discontinuous tunnels and twinned crystals.

Thermal Stability and Textural Properties of Nanosized OMS-2. TGA (Figure 6) and TPD (Figure 7) studies show that OMS-2 materials prepared with buffer solution have higher thermal stability than those obtained with HNO_3. Buffer-synthesized OMS-2 are stable up to 450 °C. When samples are heated at 500 °C, diffraction peaks corresponding to bixbyite (Mn_2O_3) begin to appear. This behavior is similar to that of the conventional OMS-2 materials. On the other hand, OMS-2 prepared with HNO_3 changes phase after calcination at 450 °C. The differences in weight loss in the range of 100−350 °C in the TGA profile of OMS-2 (1), OMS-2 (5), OMS-2 (1H), and OMS-2 (5H) reveal that samples obtained with HNO_3 are less hygroscopic than buffer-synthesized OMS-2. The marked decrease in weight loss of OMS-2 (1H) and OMS-2 (5H) after 400 °C is due to the evolution of active oxygen species. These data indicate that the oxygen release in these OMS-2 samples occurs more easily than in OMS-2 (1) and OMS-2 (5) materials. Thus, the Mn−O bond strengths are larger for OMS-2 (1) and OMS-2 (5) than their counterparts prepared with HNO_3.

The Mn−O bonding strengths of these samples can be probed by the easy release of oxygen during a TPD treatment. The TPD of O_2 for these OMS-2 materials shows mainly 2 peaks: one broad peak in the range of 400−500 °C and one sharp and intense peak around 600 °C, as observed in Figure 7. Yin et al.[36] reported similar results for OMS-2 materials prepared by reflux methods. They have classified the oxygen peaks as low-temperature (LT), medium-temperature (MT), and high-temperature (HT) peaks based on their evolution temperature. The small LT peak corresponds to weakly bound chemisorbed oxygen species. The MT peak is due to structural oxygen bound to manganese cations close to the surface, while the large HT peak corresponds to lattice oxygen. As illustrated by TPD results, the temperature regions for MT and HT oxygen peaks shift to lower values when OMS-2 is prepared with HNO_3, indicating that the nature of the acid has an effect on these peaks and on the Mn−O bond strengths. As discussed above, the tunnel structure of OMS-2 (1H) and OMS-2 (5H) remains intact up to 450 °C. At that temperature only the oxygen near the surface is desorbed, creating lattice vacancies, which are small enough to conserve the structure. At temperatures higher than 450 °C, lattice oxygen is released leading to a

(43) Vacassy, R.; Scholz, S. M.; Dutta, J.; Plummer, C. J. G.; Houriet, R.; Hoffman, H. *J. Am. Ceram. Soc.* **1998**, *81*, 2699.

(44) Post, J. E.; Veblen, D. R. *Am. Miner.* **1990**, *75*, 477.

breakdown of the structure and the formation of a new phase, Mn_2O_3. The relative intensity between MT and HT peaks is also affected by the nature of the acid used in the synthesis; however, a major effect is observed when the concentration of H_2O_2 increases. For instance, the relative intensity between MT and HT peaks for OMS-2 (5H) sample is lower than that observed for OMS-2 (1H). Similar behavior is observed in OMS-2 (1) and OMS-2 (5) samples, indicating that the lattice oxygen near the surface undergoes a major change when the amount of H_2O_2 increases.

Textural property studies show that all the nanosized OMS-2 are porous materials containing micropores, which contribute to about 2−5% of the total pore volume; mesopores, which contribute to a larger extent of the total pore volume; and also macropores are present. The pore size distribution curves of these OMS-2 nanomaterials are similar to those reported for conventional OMS-2 materials.[19] These nanomaterials exhibit a narrow pore size distribution in the micropore range with a pore diameter around 5 Å, which is close to the tunnel size of 4.6 Å for OMS-2. The BET surface area and pore volume of buffer-synthesized OMS-2 nanomaterials are higher compared to OMS-2 prepared using HNO_3. This is consistent with the particle size values obtained by XRD and HRTEM for these materials.

Catalytic Applications of Synthesized OMS-2 Nanomaterials. Nanosized OMS-2 materials prepared using the new synthetic route reported in this work were used as catalysts in the oxidation of benzyl alcohol and fluorene. Contrary to what was expected, H−K−OMS-2 (1) catalysts show 16% conversion in the oxidation of benzyl alcohol, whereas conventional H−K−OMS-2 have a conversion of 97% under the same conditions. However, this new nanomaterial shows a unique catalytic activity for the oxidation of fluorene to 9-fluorenone, for which conventional OMS-2 has poor activity. The difference in catalytic activity of nanosized OMS-2 compared to that of the conventional H−K−OMS-2 may be due to the surface properties of the materials. While conventional OMS-2 show a preferential orientation, which is usually the (110) plane, as reported in the literature,[20,33,45] HRTEM images of as-prepared OMS-2 nanomaterials suggest the presence of lattice fringes of variable dimensions, indicating the existence of different planes in the surface of the materials. The above evidence and the inability of H−K−OMS-2 (1) nanomaterial to oxide benzyl alcohol to a larger extent indicate that the planes exposed on the surface of the catalyst have an effect on the oxidative reaction. Makwana et al.[36] proved that the lattice oxygen close to the surface are directly related with the activity of the catalyst toward alcohol oxidation. Then, the poor performance of the nanosized OMS-2 in the oxidation of benzyl alcohol may be related with the changes of surface structure, such as different crystal orientation and discontinuous growth of the tunnel, which affects the availability of lattice oxygen in the surface for the reaction. On the other hand, the presence of different planes on the surface of these nanomaterials might be the reason for the high activity of OMS-2 nanomaterials for the oxidation of fluorene without the use of H_2O_2 or other initiators. The existence of oxygen vacancies due to the crystal defects observed by HRTEM may be another reason for the excellent activity of the materials in the catalytic oxidation of fluorene. Further investigations of the mechanism of the catalytic reaction for nanosized OMS-2 materials are ongoing.

(45) Yamamoto. S.; Matsuoka, O.; Fukada, I.; Ashida, Y.; Honda, T.; Yamamoto, N. *J. Catal.* **1996**, *159*, 401.

V. Conclusions

Cryptomelane-type manganese oxide (OMS-2) nanofibers with particle sizes (crystallite sizes and fiber width) as small as 6 nm were successfully synthesized by H_2O_2 reduction method for the first time. This new method is simple, eliminates the use of Mn^{2+} source, and reduces the synthesis time. Concentration of H_2O_2 plays an important role in the crystal growth and controlled particle size of the nanostructured crystals. The nature of the acid used also has an effect on the formation process of the cryptomelane-type materials and the thermal stability of the final product. Acetate groups from the buffer solution act as complexing agents preventing the growth of the particles during the formation process, whereas nitric acid reduces the reduction potential of the system due to its oxidative nature. These nanomaterials show different crystal orientation and microstructure compared to conventional OMS-2 materials, as shown by HRTEM. The acid form of nanosized OMS-2 materials show exceptional catalytic activity in the oxidation of fluorene to the corresponding ketone if compared with conventional OMS-2 catalyst. However, the activity of these nanomaterials toward alcohol oxidation decreases, which is related to the change in the surface structure of the materials.

Acknowledgment. We acknowledge support by the Geosciences and Biosciences Division, Office of Basic Energy Sciences, Office of Science, U.S. Department of Energy. We also thank to Dr. Mark Aindow for use of the JEOL 2010 TEM in the Institute of Materials Science, University of Connecticut, and Mr. James Romanow for use of the FESEM in the Geophysics and Biology Department. Special thanks to Dr. Oscar Giraldo for helpful suggestions and discussions.

CM048391U